

Blind Calibration for Acoustic Vector Sensor Arrays

Ramamohan, Krishnaprasad Nambur; Chepuri, Sundeep Prabhakar; Comesana, Daniel Fernandez; Pousa, Graciano Carrillo; Leus, Geert

DOI

[10.1109/ICASSP.2018.8462035](https://doi.org/10.1109/ICASSP.2018.8462035)

Publication date

2018

Document Version

Final published version

Published in

2018 IEEE International Conference on Acoustics, Speech, and Signal Processing, ICASSP 2018 - Proceedings

Citation (APA)

Ramamohan, K. N., Chepuri, S. P., Comesana, D. F., Pousa, G. C., & Leus, G. (2018). Blind Calibration for Acoustic Vector Sensor Arrays. In *2018 IEEE International Conference on Acoustics, Speech, and Signal Processing, ICASSP 2018 - Proceedings* (pp. 3544-3548). Article 8462035 IEEE. <https://doi.org/10.1109/ICASSP.2018.8462035>

Important note

To cite this publication, please use the final published version (if applicable). Please check the document version above.

Copyright

Other than for strictly personal use, it is not permitted to download, forward or distribute the text or part of it, without the consent of the author(s) and/or copyright holder(s), unless the work is under an open content license such as Creative Commons.

Takedown policy

Please contact us and provide details if you believe this document breaches copyrights. We will remove access to the work immediately and investigate your claim.

Green Open Access added to TU Delft Institutional Repository

'You share, we take care!' - Taverne project

<https://www.openaccess.nl/en/you-share-we-take-care>

Otherwise as indicated in the copyright section: the publisher is the copyright holder of this work and the author uses the Dutch legislation to make this work public.

BLIND CALIBRATION FOR ACOUSTIC VECTOR SENSOR ARRAYS

Krishnaprasad Nambur Ramamohan ^{†,‡}, Sundeep Prabhakar Chepuri [†], Daniel Fernández Comesaña [‡],
Graciano Carrillo Pousa [‡] and Geert Leus [†]

[†] Delft University of Technology, Delft, The Netherlands
[‡] Microflow Technologies, 6824 BV Arnhem, The Netherlands

ABSTRACT

In this paper, we present a calibration algorithm for acoustic vector sensors arranged in a uniform linear array configuration. To do so, we do not use a calibrator source, instead we leverage the Toeplitz blocks present in the data covariance matrix. We develop linear estimators for estimating sensor gains and phases. Further, we discuss the differences of the presented blind calibration approach for acoustic vector sensor arrays in comparison with the approach for acoustic pressure sensor arrays. In order to validate the proposed blind calibration algorithm, simulation results for direction-of-arrival (DOA) estimation with an uncalibrated and calibrated uniform linear array based on minimum variance distortion less response and multiple signal classification algorithms are presented. The calibration performance is analyzed using the Cramér-Rao lower bound of the DOA estimates.

Index Terms— Acoustic vector sensor, direction-of-arrival estimation, gain estimation, phase estimation, self calibration.

1. INTRODUCTION

Direction-of-arrival (DOA) estimation of outdoor acoustic sources using a network of passive sensors is crucial for ground surveillance [1] and target tracking [2]. Traditionally, microphone/acoustic pressure sensor (APS) arrays are deployed for such tasks. However, with the advances in the sensor technology, transducers that are capable of measuring vector quantities such as particle velocity are becoming practically feasible [3–5]. An acoustic vector sensor (AVS) is one such device that can measure both acoustic pressure and particle velocity at a given spatial location [6, 7]. It comprises of an omni-directional microphone and two (or three) particle velocity transducers each aligned along the coordinate axes either in \mathbb{R}^2 (or \mathbb{R}^3) [5]. An array of AVSs has several advantages compared to an equivalent aperture APS array [6, 8].

For DOA estimation using spatially distributed AVS or APS arrays, many advanced algorithms that yield highly accurate estimates are developed, such as minimum variance distortionless response (MVDR) beamformer [9] and subspace-based methods like multiple signal classification (MUSIC) [10]. However, these algorithms are highly sensitive to sensor position errors, bearing errors, and other modeling parameters such as relative gain and phase variations within as well as among sensors. Although with proper care while building the array the positional and bearing errors can be minimized, modeling parameters usually vary with time and environmental conditions. Therefore, the array has to be calibrated from

This work is part of the ASPIRE project (project 14926 within the STW OTP programme), which is financed by the Netherlands Organization for Scientific Research (NWO).

time to time. In this paper, we focus on gain and phase calibration of AVS arrays.

Currently, sophisticated calibration techniques are employed to correct for the gain and phase mismatch between the pressure and particle velocity channels [11, 12], e.g., using a calibrator source in a controlled environment. The data acquisition electronics (e.g., oscillator and amplifier) of the AVS drifts over period of time and it requires recalibration. Also, the lack of orthogonality between the channels of the particle velocity transducers contribute to the gain and phase mismatch. This means that a calibrator source has to be deployed in the field or the AVSs in the array have to be brought back to the calibration room. To avoid such complications, we explore calibrator-source-free or blind calibration techniques for AVS arrays arranged in a uniform linear array (ULA) configuration. The presented approach is inspired by the blind calibration method for APS ULA presented in [13], wherein the Toeplitz structure in the covariance matrix was utilized. An extension of this approach to any arbitrary array configuration was presented in [15]. Even though the covariance matrix of the AVS ULA is not Toeplitz, it has Toeplitz blocks. Due to which, the AVS array cannot be treated as an APS array with a larger aperture for calibration. We exploit the structure in the Covariance matrix to create a linear system of equations to estimate the unknown gain and phase uncertainties. Also, we will discuss the differences between the calibration algorithm for AVS arrays and APS arrays, which is a rather well-studied problem. Once the gain and phase uncertainties are corrected for, any standard DOA estimation technique can be employed.

2. SYSTEM MODEL

Consider a ULA of M AVSs. Each AVS consists of three elements (one pressure and two particle velocity transducers), which we denote with the subscripts \mathcal{P} , \mathcal{X} , and \mathcal{Y} throughout this paper. With the notation, $\mathbf{A}_{\mathcal{M}}$ for $\mathcal{M} \in \{\mathcal{P}, \mathcal{X}, \mathcal{Y}\}$, we mean $\mathbf{A}_{\mathcal{P}}$, $\mathbf{A}_{\mathcal{X}}$, and $\mathbf{A}_{\mathcal{Y}}$, respectively.

Let us denote the *unknown* gain and phase parameters as $\boldsymbol{\psi} \in \mathbb{R}^{3M}$ and $\boldsymbol{\phi} \in \mathbb{C}^{3M}$, respectively, where these vectors have components related to the transducers in the array, i.e.,

$$\boldsymbol{\psi} = [\boldsymbol{\psi}_{\mathcal{P}}^T, \boldsymbol{\psi}_{\mathcal{X}}^T, \boldsymbol{\psi}_{\mathcal{Y}}^T]^T, \quad \text{and} \quad \boldsymbol{\phi} = [\boldsymbol{\phi}_{\mathcal{P}}^T, \boldsymbol{\phi}_{\mathcal{X}}^T, \boldsymbol{\phi}_{\mathcal{Y}}^T]^T,$$

with length- M vectors $\boldsymbol{\psi}_{\mathcal{M}} = [\psi_{\mathcal{M},1} \dots \psi_{\mathcal{M},M}]^T$ and $\boldsymbol{\phi}_{\mathcal{M}} = [e^{j\phi_{\mathcal{M},1}} \dots e^{j\phi_{\mathcal{M},M}}]^T$ denoting the gain and phase vectors related to the type- \mathcal{M} transducer in the array.

Assume that there are D far-field narrowband uncorrelated sources with wavenumber $k = 2\pi/\lambda$ impinging on the array from azimuth angles $\boldsymbol{\theta} = [\theta_1 \ \theta_2 \ \dots \ \theta_D]^T \in \mathbb{R}^{D \times 1}$. The received signal

can be collected in $\mathbf{r}(t) \in \mathbb{C}^{3M \times 1}$ and is given by

$$\mathbf{r}(t) = \text{diag}(\boldsymbol{\psi}) \text{diag}(\boldsymbol{\phi}) [\mathbf{A}(\boldsymbol{\theta}) \mathbf{s}(t) + \mathbf{n}(t)], \quad (1)$$

where $\mathbf{s}(t) = [s_1(t) \ s_2(t) \ \dots \ s_D(t)]^T \in \mathbb{C}^D$ is the source signal vector, $\mathbf{n}(t)$ is the noise vector, and $\mathbf{A}(\boldsymbol{\theta}) = [\mathbf{a}(\theta_1) \ \mathbf{a}(\theta_2) \ \dots \ \mathbf{a}(\theta_D)] \in \mathbb{C}^{3M \times D}$ is the array manifold matrix. The d th column of $\mathbf{A}(\boldsymbol{\theta})$ is given by the corresponding length- $3M$ AVS array steering vector

$$\begin{aligned} \mathbf{a}(\theta_d) &= [\mathbf{a}_P^T(\theta_d) \ \cos(\theta_d) \mathbf{a}_P^T(\theta_d) \ \sin(\theta_d) \mathbf{a}_P^T(\theta_d)]^T, \\ &= [\mathbf{a}_P^T(\theta_d) \ \mathbf{a}_X^T(\theta_d) \ \mathbf{a}_Y^T(\theta_d)]^T, \end{aligned}$$

with

$$\mathbf{a}_P(\theta_d) = [1 \ e^{jk_l \cos(\theta_d)} \ \dots \ e^{jk_l(M-1) \cos(\theta_d)}]^T \in \mathbb{C}^{M \times 1},$$

being the equivalent APS array steering vector. Here, l is the inter-element spacing.

In this work, we assume that $\mathbf{s}(t)$ and $\mathbf{n}(t)$ are uncorrelated, and that they are realizations of an independent and identically distributed (i.i.d.) complex Gaussian process with zero mean and unknown covariance matrix $\mathbf{R}_s = \mathbb{E}\{\mathbf{s}(t)\mathbf{s}^H(t)\}$ and $\mathbf{R}_n = \mathbb{E}\{\mathbf{n}(t)\mathbf{n}^H(t)\}$, respectively. Without loss of generality, we assume that \mathbf{R}_s is a diagonal matrix with unknown entries (i.e., sources are uncorrelated) and $\mathbf{R}_n = \sigma_n^2 \mathbf{I}$ (i.e., we absorb the factor that models the noise difference between the pressure and velocity channels [16] in the calibration parameters).

The data covariance matrix $\mathbf{R} = \mathbb{E}\{\mathbf{r}(t)\mathbf{r}^H(t)\} \in \mathbb{C}^{3M \times 3M}$ can be written as

$$\mathbf{R} = \text{diag}(\boldsymbol{\psi}) \text{diag}(\boldsymbol{\phi}) \mathbf{Q} \text{diag}(\boldsymbol{\phi}^*) \text{diag}(\boldsymbol{\psi}), \quad (2)$$

where $(\cdot)^*$ denotes complex conjugation and $\mathbf{Q} = \mathbf{A}(\boldsymbol{\theta}) \mathbf{R}_s \mathbf{A}^H(\boldsymbol{\theta}) + \mathbf{R}_n$. The covariance matrices \mathbf{Q} and \mathbf{R} comprises blocks of matrices as

$$\mathbf{R} = \begin{bmatrix} \mathbf{R}_{\mathcal{P}\mathcal{P}} & \mathbf{R}_{\mathcal{P}\mathcal{X}} & \mathbf{R}_{\mathcal{P}\mathcal{Y}} \\ \mathbf{R}_{\mathcal{X}\mathcal{P}} & \mathbf{R}_{\mathcal{X}\mathcal{X}} & \mathbf{R}_{\mathcal{X}\mathcal{Y}} \\ \mathbf{R}_{\mathcal{Y}\mathcal{P}} & \mathbf{R}_{\mathcal{Y}\mathcal{X}} & \mathbf{R}_{\mathcal{Y}\mathcal{Y}} \end{bmatrix}; \quad \mathbf{Q} = \begin{bmatrix} \mathbf{Q}_{\mathcal{P}\mathcal{P}} & \mathbf{Q}_{\mathcal{P}\mathcal{X}} & \mathbf{Q}_{\mathcal{P}\mathcal{Y}} \\ \mathbf{Q}_{\mathcal{X}\mathcal{P}} & \mathbf{Q}_{\mathcal{X}\mathcal{X}} & \mathbf{Q}_{\mathcal{X}\mathcal{Y}} \\ \mathbf{Q}_{\mathcal{Y}\mathcal{P}} & \mathbf{Q}_{\mathcal{Y}\mathcal{X}} & \mathbf{Q}_{\mathcal{Y}\mathcal{Y}} \end{bmatrix},$$

where

$$\mathbf{R}_{\mathcal{M}\mathcal{N}} = \text{diag}(\boldsymbol{\psi}_{\mathcal{M}}) \text{diag}(\boldsymbol{\phi}_{\mathcal{M}}) \mathbf{Q}_{\mathcal{M}\mathcal{N}} \text{diag}(\boldsymbol{\phi}_{\mathcal{N}}^*) \text{diag}(\boldsymbol{\psi}_{\mathcal{N}}); \quad (3)$$

$$\mathbf{Q}_{\mathcal{M}\mathcal{N}} = \sum_{d=1}^D [\mathbf{R}_s]_{dd} \mathbf{a}_{\mathcal{M}}(\theta_d) \mathbf{a}_{\mathcal{N}}^H(\theta_d) + \sigma_n^2 \mathbf{I}, \quad (4)$$

for $\mathcal{M}, \mathcal{N} \in \{\mathcal{P}, \mathcal{X}, \mathcal{Y}\}$ are each Toeplitz.

In practice, the true covariance matrix is not available and we have to use a sample covariance matrix, which is evaluated from a finite number of time snapshots, N , as

$$\hat{\mathbf{R}} = \frac{1}{N} \sum_{t=1}^N \mathbf{r}(t) \mathbf{r}^H(t). \quad (5)$$

For the sake of brevity, henceforth we simply use \mathbf{R} instead of $\hat{\mathbf{R}}$. In what follows, we present linear estimators for $\boldsymbol{\psi}$ and $\boldsymbol{\phi}$ by taking into account the structure of the covariance matrix.

3. ESTIMATION OF SENSOR GAINS

In this section, we derive a least-squares estimator for $\boldsymbol{\psi}$. To do so, we process each subblock of the data covariance matrix separately to build a linear system of equations in $\boldsymbol{\psi}$. From (3), we have

$$|[\mathbf{R}_{\mathcal{M}\mathcal{N}}]_{ij}| = |[\mathbf{Q}_{\mathcal{M}\mathcal{N}}]_{ij}| \psi_{\mathcal{M},i} \psi_{\mathcal{N},j}, \quad \forall i, j = 1, 2, \dots, M, \quad (6)$$

where $|\cdot|$ denotes the modulus. Since the subblock $\mathbf{Q}_{\mathcal{M}\mathcal{N}}$ is Toeplitz, we have, for all $i - j = k - l$, the following relation

$$\begin{aligned} \log\left(\frac{|[\mathbf{R}_{\mathcal{M}\mathcal{N}}]_{ij}|}{|[\mathbf{R}_{\mathcal{M}\mathcal{N}}]_{kl}|}\right) &= \log(\psi_{\mathcal{M},i}) + \log(\psi_{\mathcal{N},j}) \\ &\quad - \log(\psi_{\mathcal{M},k}) - \log(\psi_{\mathcal{N},l}). \end{aligned} \quad (7)$$

This is because, for all $i - j = k - l$, $|[\mathbf{R}_{\mathcal{M}\mathcal{N}}]_{ij}|$ and $|[\mathbf{R}_{\mathcal{M}\mathcal{N}}]_{kl}|$ lie along the same diagonal and due to the Toeplitz structure of the subblock $\mathbf{Q}_{\mathcal{M}\mathcal{N}}$, those terms are eliminated resulting in an equation corresponding to the unknown gains. However, when only a finite number of snapshots are available, (7) is not consistent. Now, we can collect the measurements $\{\log(|[\mathbf{R}_{\mathcal{M}\mathcal{N}}]_{ij}|) - \log(|[\mathbf{R}_{\mathcal{M}\mathcal{N}}]_{kl}|), \forall i - j = k - l\}$ in the vector $\mathbf{g}_{\mathcal{M}\mathcal{N}}$, and repeat the same procedure for all the subblocks in \mathbf{R} .

Taking all the non-redundant relations within the diagonal subblocks $\mathbf{R}_{\mathcal{P}\mathcal{P}}$, $\mathbf{R}_{\mathcal{X}\mathcal{X}}$, and $\mathbf{R}_{\mathcal{Y}\mathcal{Y}}$, we get a total of $k_{z1} = 3 \sum_{i=2}^M 0.5 i(i-1)$ equations, while taking the upper-diagonal subblocks along the $\mathbf{R}_{\mathcal{P}\mathcal{X}}$, $\mathbf{R}_{\mathcal{P}\mathcal{Y}}$, and $\mathbf{R}_{\mathcal{X}\mathcal{Y}}$, we get $k_{z2} = 3(\sum_{i=2}^M 0.5 i(i-1) + \sum_{i=2}^{M-1} 0.5 i(i-1))$ equations. In total, we have $k_z = k_{z1} + k_{z2}$ equations, which can be compactly written as

$$\begin{bmatrix} \mathbf{g}_{\mathcal{P}\mathcal{P}} \\ \mathbf{g}_{\mathcal{X}\mathcal{X}} \\ \mathbf{g}_{\mathcal{Y}\mathcal{Y}} \\ \mathbf{g}_{\mathcal{P}\mathcal{X}} \\ \mathbf{g}_{\mathcal{P}\mathcal{Y}} \\ \mathbf{g}_{\mathcal{X}\mathcal{Y}} \end{bmatrix} = \begin{bmatrix} \mathbf{H}_1 & \mathbf{0} & \mathbf{0} \\ \mathbf{0} & \mathbf{H}_1 & \mathbf{0} \\ \mathbf{0} & \mathbf{0} & \mathbf{H}_1 \\ \mathbf{H}_2 & \mathbf{H}_3 & \mathbf{0} \\ \mathbf{H}_2 & \mathbf{0} & \mathbf{H}_3 \\ \mathbf{0} & \mathbf{H}_2 & \mathbf{H}_3 \end{bmatrix} \begin{bmatrix} \tilde{\boldsymbol{\psi}}_{\mathcal{P}} \\ \tilde{\boldsymbol{\psi}}_{\mathcal{X}} \\ \tilde{\boldsymbol{\psi}}_{\mathcal{Y}} \end{bmatrix} \Leftrightarrow \mathbf{g} = \mathbf{H} \tilde{\boldsymbol{\psi}}, \quad (8)$$

where $\mathbf{H} \in \mathbb{R}^{k_z \times 3M}$ and $\tilde{\boldsymbol{\psi}}_{\mathcal{M}} = [\log(\psi_{\mathcal{M},1}) \ \dots \ \log(\psi_{\mathcal{M},M})]^T$ for $\mathcal{M} \in \{\mathcal{P}, \mathcal{X}, \mathcal{Y}\}$ are each of length M .

The rows of \mathbf{H}_1 have one of the following forms [13]:

1. $[\dots 020 \dots 0 - 20 \dots]$ when $i = j$ and $k = l$. All the elements in this row are zero except for a 2 and -2 at the i th and k th positions, respectively.
2. $[\dots 010 \dots 0 - 10 \dots]$ when $i \neq j$ and $j = k$. All the elements in this row are zero except for a 1 and -1 at the i th and l th positions, respectively.
3. $[\dots 010 \dots 010 \dots 0 - 10 \dots 0 - 10 \dots]$ when i, j, k and l are distinct. All the elements in this row are zero except for 1, 1, -1 and -1 at the i th, j th, k th, and l th positions, respectively.

The rows of \mathbf{H}_2 and \mathbf{H}_3 have one of the following forms:

1. All the elements in the rows of \mathbf{H}_2 are zero except for a 1 and -1 at the i th and k th positions, respectively, and they will be of the form $[\dots 010 \dots 0 - 10 \dots]$.
2. All the elements in the rows of \mathbf{H}_3 are zero except for a 1 and -1 at the j th and l th positions, respectively, and they will be of the form $[\dots 010 \dots 0 - 10 \dots]$.

It is easy to see that the matrices \mathbf{H}_1 , \mathbf{H}_2 , and \mathbf{H}_3 each have the all-one vector $\mathbf{1}$ in its nullspace. This means that, \mathbf{H} has $3M - 3$ nonzero singular values with the vectors $[\mathbf{1}^T \ \mathbf{0}^T \ \mathbf{0}^T]^T$,

$[\mathbf{0}^T \mathbf{1}^T \mathbf{0}^T]^T$, $[\mathbf{0}^T \mathbf{0}^T \mathbf{1}^T]^T$ in its nullspace. Equations corresponding to the cross correlations between \mathcal{P} , \mathcal{X} , and \mathcal{Y} transducers, do not improve the rank of the system, but the additional equations generated from the cross blocks of \mathbf{R} might be useful to improve the estimates when only a finite number of snapshots are available.

As the matrix \mathbf{H} is not full column rank, one reference AVS with known gain is needed to uniquely determine the unknown gains. In other words, we can estimate the sensor gains $\tilde{\psi}_{\mathcal{M}}$, for $\mathcal{M} \in \{\mathcal{P}, \mathcal{X}, \mathcal{Y}\}$, up to an arbitrary multiplicative factor. To do so, let us include the known reference gains to obtain

$$\begin{bmatrix} \mathbf{g}_{\mathcal{P}\mathcal{P}} \\ \mathbf{g}_{\mathcal{X}\mathcal{X}} \\ \mathbf{g}_{\mathcal{Y}\mathcal{Y}} \\ \mathbf{g}_{\mathcal{P}\mathcal{X}} \\ \mathbf{g}_{\mathcal{P}\mathcal{Y}} \\ \mathbf{g}_{\mathcal{X}\mathcal{Y}} \\ \mathbf{0} \end{bmatrix} = \begin{bmatrix} \mathbf{H}_1 & \mathbf{0} & \mathbf{0} \\ \mathbf{0} & \mathbf{H}_1 & \mathbf{0} \\ \mathbf{0} & \mathbf{0} & \mathbf{H}_1 \\ \mathbf{H}_2 & \mathbf{H}_3 & \mathbf{0} \\ \mathbf{H}_2 & \mathbf{0} & \mathbf{H}_3 \\ \mathbf{0} & \mathbf{H}_2 & \mathbf{H}_3 \\ \hline \mathbf{e}_1^T & \mathbf{0} & \mathbf{0} \\ \mathbf{0} & \mathbf{e}_1^T & \mathbf{0} \\ \mathbf{0} & \mathbf{0} & \mathbf{e}_1^T \end{bmatrix} \begin{bmatrix} \tilde{\psi}_{\mathcal{P}} \\ \tilde{\psi}_{\mathcal{X}} \\ \tilde{\psi}_{\mathcal{Y}} \end{bmatrix} \Leftrightarrow \tilde{\mathbf{g}} = \tilde{\mathbf{H}}\tilde{\psi}, \quad (9)$$

where \mathbf{e}_1 is the first column of the identity matrix of size $M \times M$. Here, we pick, without loss of generality, the 1st AVS as the reference. Then, the sensor gains can be computed using least squares as

$$\tilde{\psi} = (\tilde{\mathbf{H}}^T \tilde{\mathbf{H}})^{-1} \tilde{\mathbf{H}}^T \tilde{\mathbf{g}}.$$

4. ESTIMATION OF SENSOR PHASES

After computing the sensor gains, in order to estimate the elements of ϕ , we again process each subblock of \mathbf{R} separately. From (3), we have

$$\text{angle}([\mathbf{R}_{\mathcal{M}\mathcal{N}}]_{ij}) = \text{angle}([\mathbf{Q}_{\mathcal{M}\mathcal{N}}]_{ij}) + \phi_{\mathcal{M},i} - \phi_{\mathcal{N},j}, \quad (10)$$

for $i, j = 1, \dots, M$. Here, $\text{angle}(\cdot)$ denotes the phase. Using the fact that each subblock $\mathbf{Q}_{\mathcal{M}\mathcal{N}}$ is Toeplitz, we obtain the relation

$$\begin{aligned} \text{angle}([\mathbf{R}_{\mathcal{M}\mathcal{N}}]_{ij}) - \text{angle}([\mathbf{R}_{\mathcal{M}\mathcal{N}}]_{kl}) &= \phi_{\mathcal{M},i} - \phi_{\mathcal{N},j} \\ &\quad - \phi_{\mathcal{M},k} + \phi_{\mathcal{N},l}, \end{aligned} \quad (11)$$

for all $i - j = k - l$. We can now collect the measurements $\{\text{angle}([\mathbf{R}_{\mathcal{M}\mathcal{N}}]_{ij}) - \text{angle}([\mathbf{R}_{\mathcal{M}\mathcal{N}}]_{kl}), \forall i - j = k - l\}$ in a vector $\mathbf{p}_{\mathcal{M}\mathcal{N}}$, and repeat the same procedure for all the subblocks in \mathbf{R} .

Taking all the nonredundant relations within the diagonal subblocks $\mathbf{R}_{\mathcal{P}\mathcal{P}}$, $\mathbf{R}_{\mathcal{X}\mathcal{X}}$, and $\mathbf{R}_{\mathcal{Y}\mathcal{Y}}$, we get $k_{p1} = 3 \sum_{i=2}^{M-1} 0.5i(i-1)$ equations while taking the upper-diagonal subblocks along the $\mathbf{R}_{\mathcal{P}\mathcal{X}}$, $\mathbf{R}_{\mathcal{P}\mathcal{Y}}$, and $\mathbf{R}_{\mathcal{X}\mathcal{Y}}$, we get a total of $k_{p2} = 3(\sum_{i=2}^M 0.5i(i-1) + \sum_{i=2}^{M-1} 0.5i(i-1))$ equations that are of the form as in (11). In total, we have $k_p = k_{p1} + k_{p2}$ equations of the form

$$\begin{bmatrix} \mathbf{p}_{\mathcal{P}\mathcal{P}} \\ \mathbf{p}_{\mathcal{X}\mathcal{X}} \\ \mathbf{p}_{\mathcal{Y}\mathcal{Y}} \\ \mathbf{p}_{\mathcal{P}\mathcal{X}} \\ \mathbf{p}_{\mathcal{P}\mathcal{Y}} \\ \mathbf{p}_{\mathcal{X}\mathcal{Y}} \\ \mathbf{0} \end{bmatrix} = \begin{bmatrix} \mathbf{G}_1 & \mathbf{0} & \mathbf{0} \\ \mathbf{0} & \mathbf{G}_1 & \mathbf{0} \\ \mathbf{0} & \mathbf{0} & \mathbf{G}_1 \\ \mathbf{H}_2 & -\mathbf{H}_3 & \mathbf{0} \\ \mathbf{H}_2 & \mathbf{0} & -\mathbf{H}_3 \\ \mathbf{0} & \mathbf{H}_2 & -\mathbf{H}_3 \\ \hline \mathbf{e}_1^T & \mathbf{0} & \mathbf{0} \\ \mathbf{0} & \mathbf{e}_1^T & \mathbf{0} \\ \mathbf{0} & \mathbf{0} & \mathbf{e}_1^T \\ \mathbf{e}_2^T & \mathbf{0} & \mathbf{0} \end{bmatrix} \begin{bmatrix} \tilde{\phi}_{\mathcal{P}} \\ \tilde{\phi}_{\mathcal{X}} \\ \tilde{\phi}_{\mathcal{Y}} \end{bmatrix} \Leftrightarrow \mathbf{p} = \tilde{\mathbf{G}}\tilde{\phi}, \quad (12)$$

where $\mathbf{G} \in \mathbb{R}^{k_p \times 3M}$ and $\tilde{\phi}_{\mathcal{M}} = [\phi_{\mathcal{M},1} \dots \phi_{\mathcal{M},M}]^T$ for $\mathcal{M} \in \{\mathcal{P}, \mathcal{X}, \mathcal{Y}\}$ are each of length M .

The rows of \mathbf{G}_1 have one of the following forms:

1. $[\dots 010 \dots 0 - 20 \dots 010 \dots]$ when $i \neq j$ and $j = k$. All the elements in this row are zero except for a 1, -2 and 1 at the i th, $j(=k)$ th, and the l th positions, respectively.
2. $[\dots 010 \dots 0 - 10 \dots 0 - 10 \dots 010 \dots]$ when i, j, k and l are distinct. All the elements in this row are zero except for 1, -1, -1, and 1 at the i th, j th, k th and l th positions, respectively.

The matrix \mathbf{G}_1 has $M - 2$ nonzero singular values and there are two $M \times 1$ vectors, namely, $[11 \dots 1]^T$ and $[12 \dots M]^T$ in its nullspace. However, \mathbf{G} has $3M - 4$ nonzero singular values with four $3M \times 1$ vectors in its nullspace. Those include $[\mathbf{1}^T \mathbf{0}^T \mathbf{0}^T]^T$, $[\mathbf{0}^T \mathbf{1}^T \mathbf{0}^T]^T$, $[\mathbf{0}^T \mathbf{0}^T \mathbf{1}^T]^T$, and $[\mathbf{t}^T \mathbf{t}^T \mathbf{t}^T]^T$, where $\mathbf{t} = [123 \dots M]^T$. By exploiting the cross correlations between \mathcal{P} , \mathcal{X} , and \mathcal{Y} channels, we gain rank, i.e., the rank is increased to $3M - 4$ from $3M - 6$. This is the main advantage of jointly performing the phase calibration for all the transducer types in the AVS array.

To solve (12), when \mathcal{P} , \mathcal{X} , and \mathcal{Y} channels are processed independently (i.e., without considering the equations related to the cross correlations between the channels), we would require two reference AVSs. In contrast, by considering entire \mathbf{G} , we need only one reference AVS and an additional phase reference (it could be any transducer type), as its rank is $3M - 4$. Those known phase references are included as additional equations to obtain

$$\begin{bmatrix} \mathbf{p}_{\mathcal{P}\mathcal{P}} \\ \mathbf{p}_{\mathcal{X}\mathcal{X}} \\ \mathbf{p}_{\mathcal{Y}\mathcal{Y}} \\ \mathbf{p}_{\mathcal{P}\mathcal{X}} \\ \mathbf{p}_{\mathcal{P}\mathcal{Y}} \\ \mathbf{p}_{\mathcal{X}\mathcal{Y}} \\ \mathbf{0} \end{bmatrix} = \begin{bmatrix} \mathbf{G}_1 & \mathbf{0} & \mathbf{0} \\ \mathbf{0} & \mathbf{G}_1 & \mathbf{0} \\ \mathbf{0} & \mathbf{0} & \mathbf{G}_1 \\ \mathbf{H}_2 & -\mathbf{H}_3 & \mathbf{0} \\ \mathbf{H}_2 & \mathbf{0} & -\mathbf{H}_3 \\ \mathbf{0} & \mathbf{H}_2 & -\mathbf{H}_3 \\ \hline \mathbf{e}_1^T & \mathbf{0} & \mathbf{0} \\ \mathbf{0} & \mathbf{e}_1^T & \mathbf{0} \\ \mathbf{0} & \mathbf{0} & \mathbf{e}_1^T \\ \mathbf{e}_2^T & \mathbf{0} & \mathbf{0} \end{bmatrix} \begin{bmatrix} \tilde{\phi}_{\mathcal{P}} \\ \tilde{\phi}_{\mathcal{X}} \\ \tilde{\phi}_{\mathcal{Y}} \end{bmatrix} \Leftrightarrow \tilde{\mathbf{p}} = \tilde{\mathbf{G}}\tilde{\phi}, \quad (13)$$

where \mathbf{e}_1 and \mathbf{e}_2 are, respectively, the first and second columns of the identity matrix of size $M \times M$. Then, the sensor phases can be computed using least squares as

$$\tilde{\phi} = (\tilde{\mathbf{G}}^T \tilde{\mathbf{G}})^{-1} \tilde{\mathbf{G}}^T \tilde{\mathbf{p}}.$$

5. SIMULATIONS

In this section, we present numerical simulations to illustrate the developed theory. We consider an array consisting of six AVSs arranged in an ULA configuration with an inter-element spacing of $\lambda/2$. Further, the first AVS is considered as a reference with its channels having a nominal gain of 1 and a nominal phase to be 0. For solving (13), it is considered that the pressure channel of the first and second AVS as phase reference. We assume five equal-powered sources at DOAs $\theta = [-35^\circ, 68^\circ, 79^\circ, -128^\circ, 137^\circ]^T$.

The spectral plot of the MVDR and MUSIC algorithm are presented in Figure 1 and 2. Here, we use a signal-to-noise ratio of 0 dB with respect to the source signal and the sample covariance matrix $\hat{\mathbf{R}}$ is formed using $N = 1000$ snapshots. Further, up to 4 dB and 20° (root-mean-square values) of random gain and phase uncertainties with respect to the nominal values, are chosen. For MUSIC, without gain and phase uncertainties the peaks in the spectrum are in the direction of the actual sources (as indicated by dash-dotted black color line and referred to as Ideal). For MVDR without the gain and

phase uncertainties, the peaks in the spectrum are in the direction of the actual sources, however, two closely spaced sources at 68° and 79° are not resolved. When the sensors are not calibrated, it can be clearly seen that the DOA estimates are poor and the angular spectral resolution is degraded due to the sensor errors. This plot also shows that both MVDR and MUSIC are highly sensitive to the sensor errors. By following the procedure discussed in this work to estimate the sensor errors, which are then compensated during the calibration step, we can clearly see the improved spectral resolution. It is evident that the sources located at -35° , -128° , 137° are well resolved and with less bias using both MUSIC and MVDR. Further, the MUSIC algorithm can even resolve the two closely spaced sources at 68° and 79° .

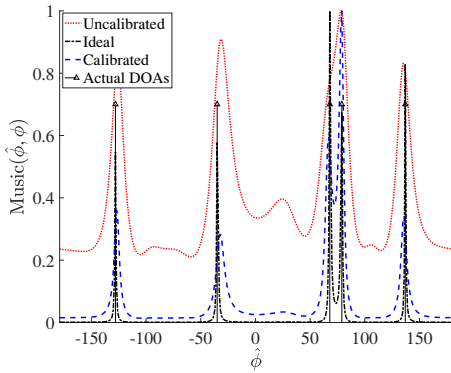


Fig. 1. Angular spectrum with, without, and after resolving sensor errors using MUSIC algorithm (here, Ideal refers to the scenario without calibration errors).

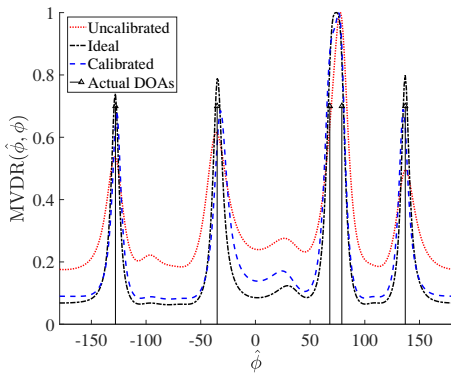


Fig. 2. Angular spectrum with, without, and after resolving sensor errors using MVDR.

In order to analyze the performance of the proposed blind calibration algorithm, the root mean squared error (RMSE) variation of the DOA estimates using MUSIC and MVDR are considered for a single source scenario through Monte Carlo experiments for a fixed gain and phase parameters. Firstly, the RMSE variation of the DOA estimates corresponding to the uncalibrated and calibrated AVS ULA are plotted for different SNRs in Fig. 3. Also, the RMSE variation of the AVS ULA without sensor errors and the Cramér-Rao lower bound (CRB) are plotted in Fig. 3. For each SNR value, the

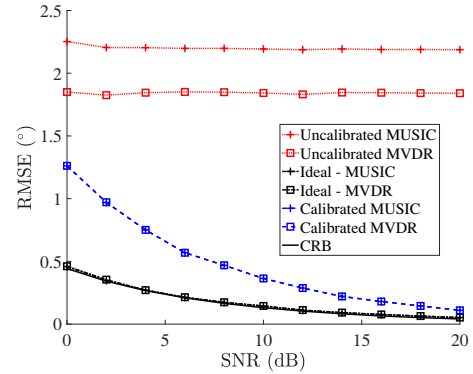


Fig. 3. RMSE variation of the DOA estimate for increasing SNR using AVS ULA under single source scenario with $M = 3$, $\theta = 60^\circ$ and $N = 300$.

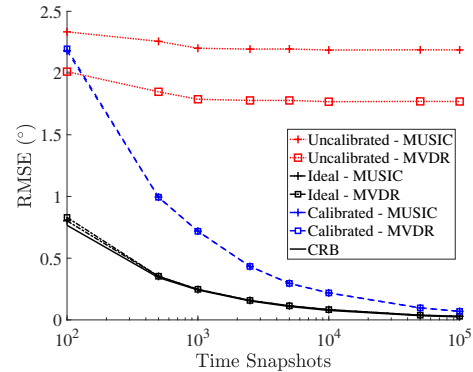


Fig. 4. RMSE variation of the DOA estimate for increasing number of time snapshots (N) using AVS ULA under single source scenario with $M = 3$, $\theta = 60^\circ$ and SNR = 0 dB.

RMSE value is evaluated using 1000 independent trials. It is observed that as the SNR increases, the RMSE of the DOA estimates for both MUSIC and MVDR of the calibrated ULA approaches to the ideal AVS ULA and the CRB. However, the RMSE of DOA estimates of the uncalibrated ULA does not improve with the SNR.

Finally, in Fig. 4, the RMSE variation of the DOA estimates using both MUSIC and MVDR for increasing number of snapshots is shown. Again for evaluating the RMSE values, 1000 Monte Carlo experiments were performed. A similar observation as in Fig. 3 can be made, where the calibrated array achieves the CRB as the number of snapshots increase. In a nut shell, the DOA estimates after the proposed calibration are asymptotically (with SNR and/or number of snapshots) efficient as they achieve the CRB.

6. CONCLUDING REMARKS

In this paper, we estimate the sensor errors present in the AVS ULA by exploiting the structure in the covariance matrix. In particular, we derived linear estimators for sensor gains and phases. The proposed calibration algorithm does not require a calibrator source, and being a blind algorithm, the unknown gains and phases are estimated relative to a reference sensor. To validate the proposed approach, simulations performed with MUSIC and MVDR for DOA estimation show a significant improvement after calibration.

7. REFERENCES

- [1] H.-E. de Bree, J. Wind, and E. Tijs, "Environmental noise monitoring with acoustic vector sensors," in *INTER-NOISE and NOISE-CON Congress and Conference Proceedings*, vol. 2010, no. 5. Institute of Noise Control Engineering, 2010, pp. 6225–6231.
- [2] H.-E. de Bree, J. Wind, and P. de Theije, "Detection, localization and tracking of aircraft using acoustic vector sensors," *Inter Noise 2011 Proceedings, Osaka, Japan*, pp. 4–7, 2011.
- [3] H.-E. de Bree, "An overview of microflown technologies," *Acta acustica united with Acustica*, vol. 89, no. 1, pp. 163–172, 2003.
- [4] H.-E. Bree, P. Leussink, T. Korthorst, H. Jansen, T. Lamerink, and M. Elwenspoek, "The μ -flown: A novel device measuring acoustical flows," 1995.
- [5] H.-E. De Bree, "The microflown e-book," *Microflown Technologies, Arnhem*, 2007.
- [6] A. Nehorai and E. Paldi, "Acoustic vector-sensor array processing," *IEEE Transactions on Signal Processing*, vol. 42, no. 9, pp. 2481–2491, 1994.
- [7] J. P. Kitchens, "Acoustic vector-sensor array processing," Ph.D. dissertation, Massachusetts Institute of Technology, 2010.
- [8] M. Hawkes and A. Nehorai, "Effects of sensor placement on acoustic vector-sensor array performance," *IEEE Journal of Oceanic Engineering*, vol. 24, no. 1, pp. 33–40, 1999.
- [9] J. Capon, "High-resolution frequency-wavenumber spectrum analysis," *Proceedings of the IEEE*, vol. 57, no. 8, pp. 1408–1418, 1969.
- [10] H. L. Van Trees, *Detection, estimation, and modulation theory. Part IV. , Optimum array processing*. New York: Wiley-Interscience, 2002.
- [11] T. G. Basten and H.-E. de Bree, "Full bandwidth calibration procedure for acoustic probes containing a pressure and particle velocity sensor," *The Journal of the Acoustical Society of America*, vol. 127, no. 1, pp. 264–270, 2010.
- [12] T. Basten, J. Wind, B. Xu, H.-E. De Bree, and E. Druyvesteyn, "Amplitude, phase, location and orientation calibration of an acoustic vector sensor array, part ii: Experiments," in *Proceedings of Meetings on Acoustics 159ASA*, vol. 9, no. 1. ASA, 2010, p. 070004.
- [13] A. Paulraj and T. Kailath, "Direction of arrival estimation by eigenstructure methods with unknown sensor gain and phase," in *Acoustics, Speech, and Signal Processing, IEEE International Conference on ICASSP'85*, vol. 10. IEEE, 1985, pp. 640–643.
- [14] A. L. Swindlehurst and T. Kailath, "A performance analysis of subspace-based methods in the presence of model errors. i. the music algorithm," *IEEE Transactions on signal processing*, vol. 40, no. 7, pp. 1758–1774, 1992.
- [15] B. Friedlander and A. J. Weiss, "Eigenstructure methods for direction finding with sensor gain and phase uncertainties," in *Acoustics, Speech, and Signal Processing, 1988. ICASSP-88., 1988 International Conference on*. IEEE, 1988, pp. 2681–2684.
- [16] M. Hawkes and A. Nehorai, "Acoustic vector-sensor correlations in ambient noise," *IEEE Journal of Oceanic Engineering*, vol. 26, no. 3, pp. 337–347, 2001.